IJIE

UTHM Penerbit
Universiti Tun Hussein Onn Malaysia

INTERNATIONAL JOURNAL OF INTEGRATED ENGINEERING
ISSN: 2229-838X e-ISSN: 2600-7916

Vol. 18 No. 1 (2026) 142-154
https://publisher.uthm.edu.my/ojs/index.php/ijie

Numerical Design of a THz Metamaterial Biosensor for Early Skin and Breast Cancer Detection

Suhail Asghar Qureshi[1], Zuhairiah Zainal Abidin[1]*, Noor Azwan Shairi[2]*, Huda A. Majid[3], Hongnian Yu[4], Nurul Bashirah Ghazali[5]

[1] *Faculty of Electrical and Electronic Engineering, Universiti Tun Hussein Onn Malaysia (UTHM), 86400, Batu Pahat, MALAYSIA*
[2] *Centre for Telecommunication Research and Innovation (CeTRI), Fakulti Teknologi dan Kejuruteraan Elektronik dan Komputer (FTKEK), Universiti Teknikal Malaysia Melaka (UTeM), Melaka, MALAYSIA*
[3] *Fakulti Teknologi Kejuruteraan, Universiti Tun Hussein Onn Malaysia (UTHM), 86400, Pagoh, MALAYSIA*
[4] *School of Engineering and the Built Environment, Edinburgh Napier University, GREAT BRITAIN*
[5] *Control Software Design Department, Daikin Research and Development Sdn. Bhd. Taman Perindustrian, 60334, Persiaran 3, Bukit Rahman Putra, 47000 Sungai Buloh, Selangor, MALAYSIA*

*Corresponding Author: zuhairia@uthm.edu.my; noorazwan@utem.edu.my
DOI: https://doi.org/10.30880/ijie.2026.18.01.011

Article Info

Received: 15 December 2025
Accepted: 28 March 2026
Available online: 17 April 2026

Keywords

Metamaterial, absorber, cancer, THz, sensor

Abstract

This paper presents a high-sensitivity terahertz (THz) metamaterial absorber engineered for early-stage detection of skin and breast cancers using a full-wave simulation approach. The proposed sensor employs a hybrid square-ring geometry, achieving a base absorption rate of 51% in the unloaded state. Upon dielectric loading with biological samples, the absorption rate significantly increases up to 99% for melanoma tissue and 98% for normal breast tissue. Dielectric properties of biological samples were modelled using the Double Debye model, enabling realistic simulation of tissue-specific spectral responses. The sensor exhibits measurable resonance frequency shifts up to 48 GHz between normal and malignant samples with peak sensitivity values of 5.2 GHz/μm for melanoma, 3.7 GHz/μm for basal cell carcinoma, and 1.7 GHz/μm for breast cancer. These shifts show a linear dependence on sample thickness, highlighting the potential for severity assessment. The findings establish a simulation-based foundation for non-invasive, label-free THz diagnostic systems with promising prospects for future clinical transformations.

1. Introduction

Early and accurate disease detection remains a critical challenge, as conventional diagnostic methods are often limited by delays and inaccuracies, underscoring the need for advanced sensing technologies [1]. Similarly, the incorporation of intelligent healthcare solutions, such as Internet of Things (IoT) and Artificial Intelligence (AI) systems has been emphasised as a revolutionary route to ongoing observation and prompt action, especially in applications like the detection of skin and breast cancer [2]. In this regard, Terahertz (THz) technology, operating within the 0.1 to 10 THz frequency range, has emerged as an innovative improvement in imaging and sensing. Positioned between the infrared and microwave frequency bands, this technology has gained significant attention due to its unique capabilities. With the expansion of its applicability to various fields, such as biomedical imaging [3], security and surveillance [4], and tomography [5], THz technology has become an intriguing field. One of the primary advantages of the THz band lies in its non-ionizing nature and its ability to penetrate dielectric materials to substantial depths [6]– [8], making it highly suitable for non-destructive analysis in biomedical applications [9]. Additionally, the higher spatial resolution offered by THz frequencies surpasses that of ultrasound and microwave technologies [10], further enhancing its potential utility. THz technology has already resulted in groundbreaking advances in cancer diagnosis [11]. Its low-wavelength nature enables the detection of subtle cellular variations caused by cancer, introducing a novel and potent modality of medical imaging [12]. The author in [13] has presented the preliminary potential of THz imaging for cancer detection and hence was supported by many researches on various types of cancer. Notably, THz pulsed imaging can precisely delineate the margin of ex-vivo unstained breast tumours as demonstrated in [14]. Furthermore, the development of a highly sensitive THz nano-biosensor has further demonstrated the technology's promise in detecting cancer cells, highlighting its considerable potential [15].

While significant progress has been made, challenges remain, particularly in maintaining sensitivity when analysing samples smaller than 100 nm which dimensions below the wavelength of the THz band [16]. Several recent studies have investigated related THz-based sensing and resonator approaches [3], [12], [17], providing important context for the present work. To overcome this, researchers have focused on THz biosensors incorporating metamaterials (MMs), which offer unprecedented sensitivity in biomolecular detection, particularly for cancer diagnostics. MMs, known for their unique physical properties such as super absorption, electromagnetic stealth, and negative refractive index [18], [19], have expanded the possibilities of THz sensors in biomedical applications. MM-based THz split-ring resonators (SRRs) are among the sensitive devices in detecting viruses from small to low-density species [7]. Furthermore, THz technology has been investigated for application in the detection of cancer such as water-based metamaterials to detect skin tumours (in-vivo) [20]. The THz spectrum is very sensitive to water's changes content, and because the cancerous tissues usually show higher water contents than normal tissue it makes this spectrum particularly effective. Previous experimental studies have confirmed that cancer tissues can be detected on an MM-based THz sensor and would cause resonance frequency shifts due to the loading of substances covering the sensor surface [21]. Another highly sensitive MM THz-based sensor was proposed in [22]. The resonator sensor with a double corrugation structure was developed to improve the performance in both terms of Q-factor and sensitivity. Furthermore, this innovative method allowed the sensor to identify an analyte even when it had greater thickness effectively. In recent years, these efforts have yielded further improvements in THz cancer detection. Novel MM-based absorbers have been developed, achieving high Q-factors and exceptional sensitivity in analyte thickness measurements [23]. These absorbers have demonstrated near-perfect absorptivity, emphasizing their potential for early cancer detection, particularly for breast cancer [24].

Building on these advancements, this study aims to design a THz metamaterial absorber capable of detecting both skin and breast cancers. A circular, hollow square–shaped hybrid design is proposed in this paper for the early detection of skin and breast cancer. The dielectric properties of skin and breast cancer tissues are modelled using the double-Debye model. A detailed investigation of the THz absorber-based metamaterial sensor is presented, including its design evolution and parametric study. Furthermore, an equivalent circuit analysis of the design is conducted. The proposed design achieves an absorption peak of 51% at 1.61 THz in the absence of a sample. However, the sensor is optimized in the presence of a dielectric sample, resulting in a significantly enhanced absorption peak of 92% at 1.475 THz when a normal skin sample is introduced. This improved performance demonstrates the potential of THz metamaterial absorbers in developing cancer detection.

2. Methodology

The design and analysis of the electromagnetic (EM) wave responses in this study were conducted using CST Studio, a leading software for EM field analysis. The simulations were carried out using the Frequency Domain Solver, which utilizes the Finite Element Method (FEM)—an approach particularly well-suited for high-frequency applications and resonant structures. Fig. 1 depicts the boundary conditions applied to the metamaterial (MM) absorber. In this configuration, EM waves with an electric field aligned along the y-axis and a magnetic field along the x-axis are incident on the absorber from Port 1 along the z-axis. To evaluate the absorber's performance, the scattering parameters (S_{11} and S_{21}) were analysed, which are crucial for calculating the absorption, A = 1 – T – R, where T is the squared magnitude of S_{21}, and R is the squared magnitude of S_{11} [25].

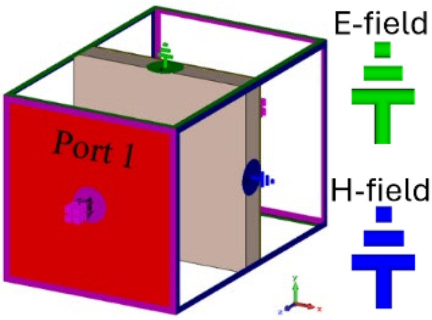

Fig. 1 *Simulation setup of the proposed THz metamaterial resonator [24]*

The design process for the proposed metamaterial absorber, particularly with the presence of a sample, was conducted in four distinct phases, as depicted in Fig. 2. The corresponding absorption properties are presented in Fig. 3. In the initial phase, a fundamental metamaterial absorber with a circular-shaped geometry was developed, as illustrated in Fig. 2(a). However, this design exhibited a relatively low absorption efficiency. To enhance the performance, a square patch was subsequently investigated, as shown in Fig. 2(b), which resulted in slightly improved absorption rate of 40%. Later, the square patch was converted into a hollow square ring (Fig. 2(c)), this resulted in an absorption rate of up to 80%. In the end, the combination of the circular shape and the square ring geometries, as depicted in Fig. 2(d), led to a significant enhancement in absorption, achieving a rate of 92%. The absorber's design features a circular structure enclosed within a square, meticulously constructed to induce electric and magnetic dipoles that generate destructive interference, thereby minimizing the reradiation of EM waves. This configuration assumes that the MM material is characterized by high ohmic losses, leading to the dissipation of EM energy as heat. The EM characteristics of the absorber are primarily governed by its geometric properties, including the diameter (d), outer length (lo), inner length (li), and the gap (g) between the circular and square shapes. A schematic of the analysed absorber is presented in Fig. 4.

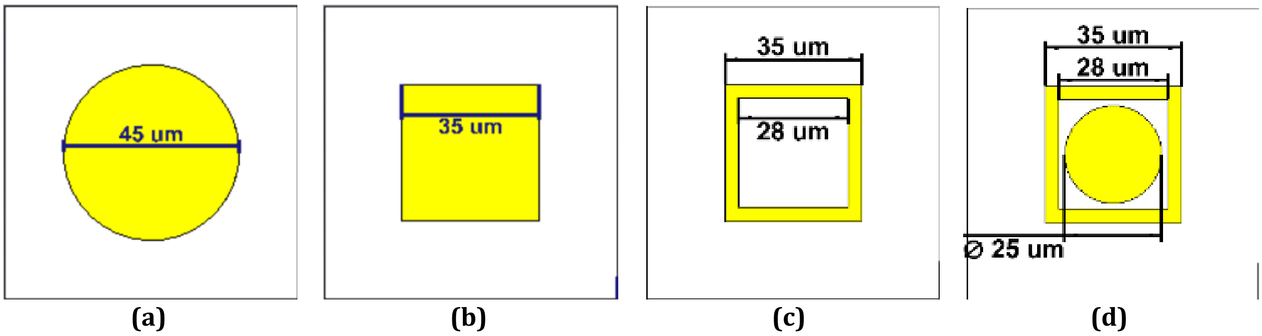

Fig. 2 *Design evolution of the proposed absorber (a) Initial circular patch design (Design 1); (b) Improved square patch (Design 2); (c) Hollow square-ring geometry (Design 3); (d) Final hybrid design combining circular and hollow square-ring geometry*

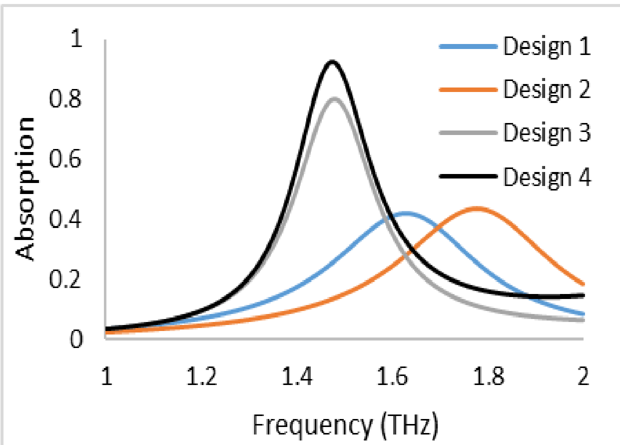

Fig. 3 *Absorption spectra of the absorber through its design evolution*

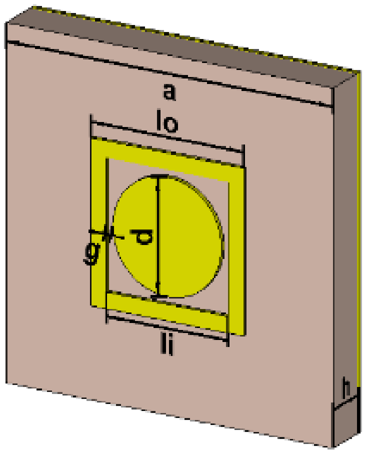

Fig. 4 *Schematic of the final absorber design*

Subsequently, the dimensions of both the square and ring geometries, along with the spacing between them, were optimized to identify the most critical parameters affecting the absorber's efficiency. Fig. 5(a) illustrates the effect of varying the diameter (d) on the absorption characteristics. Adjustments in the diameter from 23 µm to 27 µm resulted in a noticeable change in the absorption magnitude, while the operating frequency remained relatively stable. This stability is particularly crucial for applications in skin cancer detection. At a diameter of 23 µm, the absorption value was recorded at 0.88 at a frequency of 1.475 THz. An increase in diameter to 27 µm resulted in an absorption value of 0.96, accompanied by a minor frequency shift. At this larger diameter, the absorption peaked at 0.974 at a frequency of 1.767 THz. Conversely, varying the outer length (lo) from 33 µm to 37 µm induced a significant shift in the operating frequency, as demonstrated in Fig. 5(b). An increase in lo caused the absorption peak to shift towards lower frequencies. Specifically, at a length of 33 µm, an absorption peak was observed at a frequency of 1.57 THz, with an intensity of 0.95. While the absorption magnitude remained consistent, the frequency shifted towards the lower spectrum as the outer length increased to 35 µm and 37 µm.

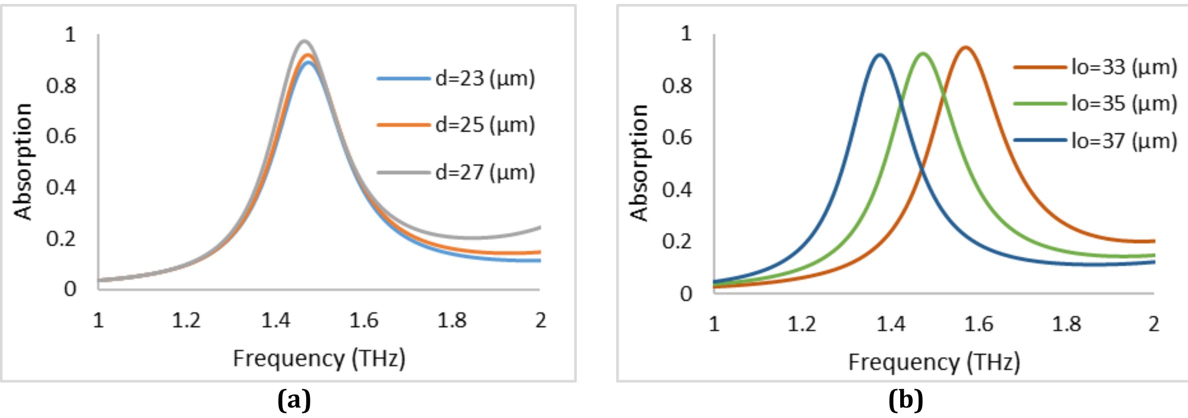

Fig. 5 *Effect of geometric variation on absorption characteristics (a) Increasing the circular diameter, d; (b) Increasing outer length, lo*

The optimised dimensions of the absorber design are detailed in Table 1. The unit cell of the proposed absorber consists of a polyimide as a substrate with a dielectric permittivity (ε) of 3.5, and a gold layer of 1 µm thickness with electrical conductivity of 4.561×10^7 S/m. Fig. 6 depicts the reflection coefficient (S_{11}) in dB, along with the absorption profile of the designed absorber. By employing the LC equivalent circuit model, the resonance frequency of the designed MM absorber was determined using (1) [17]. As illustrated in Fig. 6, the design achieves its highest absorption at 1.6 THz, with an absorption magnitude of 0.513.

$$f = \frac{1}{2\pi\sqrt{L_{eff}C_{eff}}} \qquad (1)$$

where L_{eff} is the effective inductance of the design, which is mainly contributed by the square shape and the circular resonator, whereas C_{eff} is the effective capacitance contributed by the gap between the circular resonator and the squared enclosure. Fig. 7(a) represents the RLC equivalent circuit model for the designed absorber with two segments, one representing the square ring in the design and other representing the circular patch inside the square ring. The capacitor (C3) between the two segments works as the coupling or model interaction between two segments. Fig. 7(a) draws the comparison of the reflection coefficients obtained from CST Studio and the Advanced Design System (ADS). It can be seen that the RLC values obtained from ADS as shown in Fig. 7(a) achieve very high matching with the results obtained from CST.

Table 1 *Optimized dimensions of the designed absorber*

Dimension	Value (μm)
a	75
h	10
lo	35
li	28
d	25
g	1.5

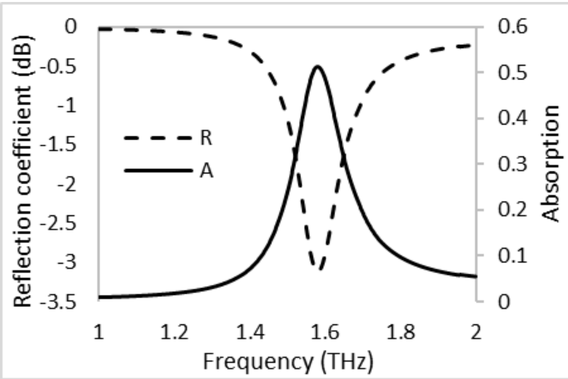

Fig. 6 *Absorption and reflection characteristic of the proposed THz MM absorber in the unloaded condition. (without biological sample)*

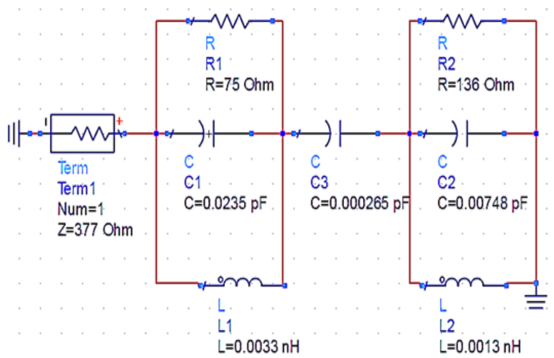

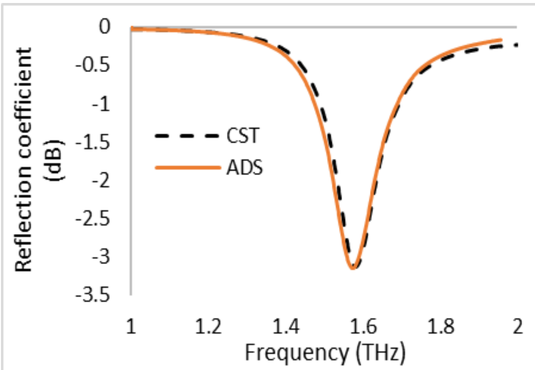

(a) **(b)**

Fig. 7 *(a) RLC equivalent circuit model representing the absorber's electromagnetic behavior, where square-ring and circular elements are modelled as coupled resonators;*
(b) Comparison between simulated and circuit-modelled reflection coefficients from CST and ADS, respectively

For the simulation of skin samples, the well-known Double Debye model was employed. Previous research has validated the use of the Double Debye theory in predicting the human skin's dielectric response in THz frequencies [26]. This approach hinges on the interaction of THz radiations with the human skin's water molecules. The Double Debye model features two relaxation processes that describe how the external electric field affects these water molecules. Natural tetrahedral structures of water molecules when exposed to incident T-rays are reoriented by the breakage and reformation of multiple hydrogen bonds besides central water molecules in the slow relaxation process [27]. This process typically occurs on the scale of picoseconds. In contrast, another relaxation process (fast relaxation) represents the reorientation of the central water molecule. The Double Debye model utilized for modelling dielectric properties of human skin is given in (2) [24].

$$\varepsilon_{r(\omega)} = \frac{\varepsilon_s - \varepsilon_2}{1 + j\omega\tau_1} + \frac{\varepsilon_2 - \varepsilon_\infty}{1 + j\omega\tau_2} \tag{2}$$

Here ε_∞ and ε_s represent the permittivity at maximum frequency and the static permittivity, respectively, ε_2 is the dielectric constant of the transition between two relaxation processes, ε_s- ε_2 represents the dispersion in amplitude of the slow relaxation process attributed to its relaxation time constant, τ_1 while ε_2- ε_∞ represent dispersion in in amplitude of fast relaxation process attributed to its relaxation time, τ_2. The double Debye parameters for the samples tested in this study are given in Table 2 [12], [28], [29].

Table 2 *Double Debye parameters of samples tested in this study*

Sample	ε_s	ε_∞	ε_2	τ_1 (ps)	τ_2 (ps)
Normal skin	25	3.4	5	7	1
BCC	40	4.2	6.2	10	1
Melanoma	58	4.3	4.6	5	0.49
Normal breast tissue	76.5	2.1	3.9	10.3	0.07
Breast cancer tissue	77.9	2.5	4.3	9.1	0.08

It is important to highlight that the sensor was specifically optimized to accommodate the introduced samples, with the primary focus on resonance behaviour upon sample placement on the absorber's surface. As depicted in Fig. 8(a), a 2 μm-thick sample (illustrated in blue) was applied to the sensor's surface. Subsequently, Fig. 8(b) demonstrates the absorption characteristics when a normal skin sample was introduced. The results indicate a leftward shift in resonance frequency (towards lower frequencies) upon the introduction of the dielectric sample. For the design optimization, a normal skin sample was employed as the reference. This led to the emergence of a new absorption peak at 1.475 THz with a substantial magnitude of 92%. To further investigate the mechanism of absorption, their electric field distribution at resonant frequency was analysed. As shown in Fig. 9, at 1.475 THz, the incident THz radiation is predominantly concentrated at the top and bottom corners of the square structure, approximately 35 μm apart. The maximum electric field magnitude was observed to be 2.37×10^7 V/m. When the skin sample was introduced, the absorption of THz radiation increased, leading to a reduction in the peak electric field magnitude to 1.97×10^7 V/m. Additionally, the introduction of the skin sample caused a reversal in the direction of the electric field pattern on the sensor's surface.

This detailed analysis of the sensor's resonance behaviour and electric field distribution underscores the meticulous optimization process, which enhances the sensor's ability to detect subtle changes in sample characteristics, thereby improving its sensitivity and effectiveness in cancer detection applications.

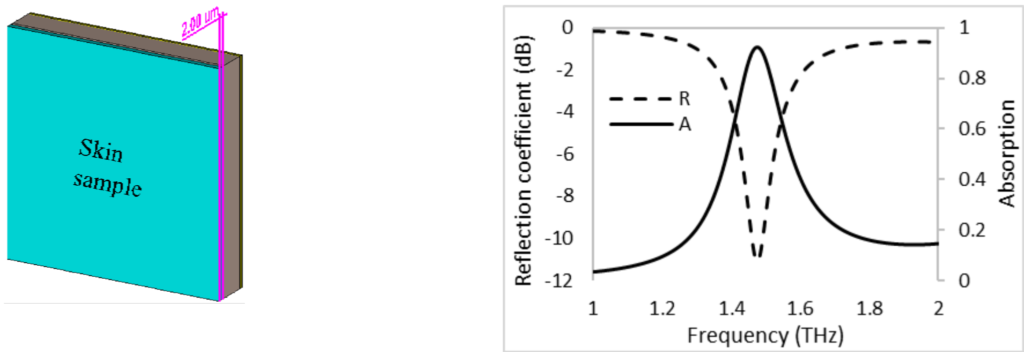

(a) **(b)**

Fig. 8 *(a) Depiction skin sample on sensor's surface; (b) Absorption and reflection characteristic sensor*

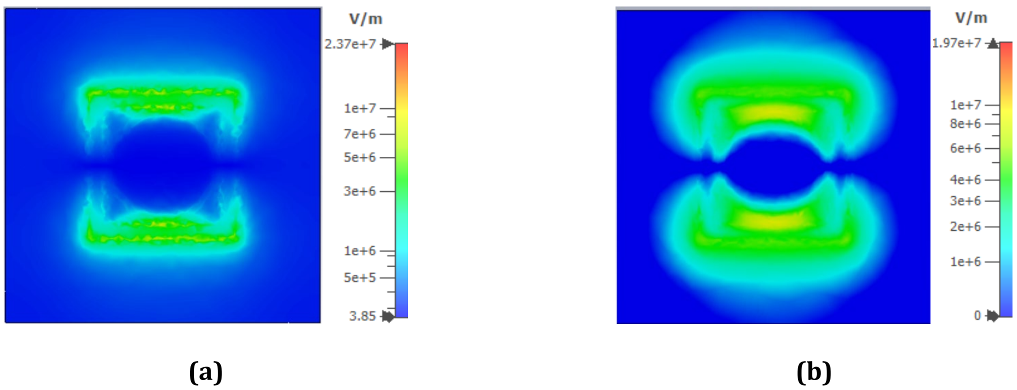

Fig. 9 *Simulated e-field distribution at the resonance frequency of 1.475 THz (a) In the absence of the biological sample; (b) Upon loading with a 2 µm-thick skin sample*

3. Results and Discussion

In this study, the sensitivity of the proposed THz sensor was evaluated for the detection of both skin and breast cancers. Initially, the sensor's performance was assessed using samples of normal skin, Basal Cell Carcinoma (BCC), and Melanoma. When the sensor was applied to suspected skin cancer, distinct shifts in the absorption spectrum were observed, indicating the presence of malignancy. As depicted in Fig. 10, a notable frequency shift to lower values occurred when cancerous skin samples were tested, with a shift of 35 GHz observed in BCC, resulting in a peak absorption at 1.44 THz, and a shift to 1.427 THz in the case of Melanoma. Moreover, the absorption magnitude increased significantly in cancerous samples, reaching 95% for BCC and 99% for Melanoma, underscoring the sensor's high sensitivity in distinguishing between healthy and malignant skin tissues.

The sensor's performance was further evaluated for breast cancer detection. In the case of normal breast tissue, the peak absorption was observed at 1.47 THz, with a high absorption rate of 98%, as depicted in Fig. 11. Consistent with the results from skin cancer detection, the introduction of cancerous breast tissue led to a downward shift in frequency, with the peak absorption moving to 1.456 THz, representing a 14 GHz shift. However, in contrast to the trend noted in skin cancer detection, the absorption rate slightly decreased when cancerous breast tissue was present, measuring at 97%.

These results highlight the significant potential of the proposed THz sensor for the precise and sensitive detection of both skin and breast cancers. The observed frequency shifts and changes in absorption underscore the sensor's effectiveness as a non-invasive diagnostic tool, offering a promising approach for early cancer diagnosis and improving clinical outcomes.

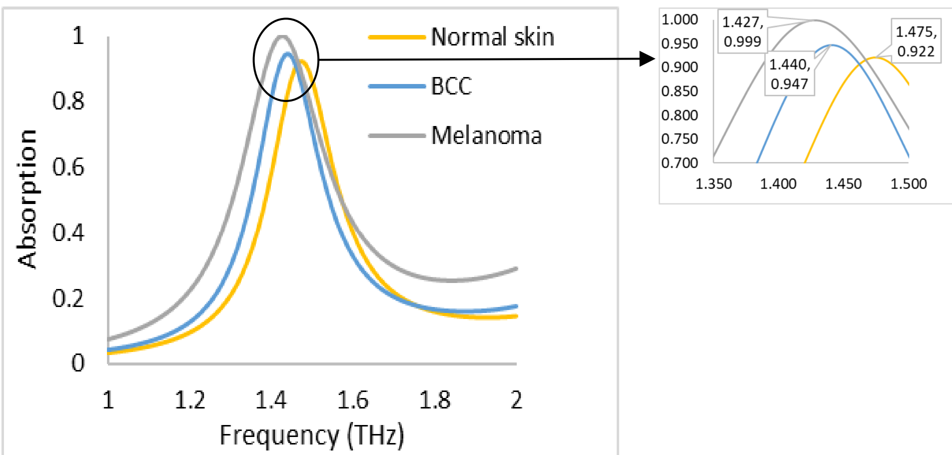

Fig. 10 *Absorption spectra for normal skin, basal cell carcinoma (BCC), and melanoma samples loaded on the absorber*

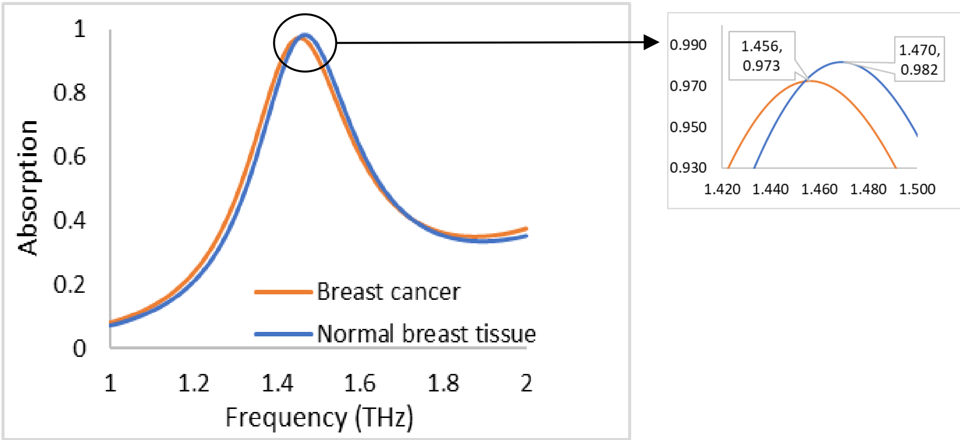

Fig. 11 *Absorption spectra for normal and breast cancer samples loaded on the absorber*

Quality-factor (Q) can be used to characterise the sensing quality of the designed sensor. Quality-factor is defined by (3) [30]:

$$Q = \frac{f_r}{\Delta f}, \quad (3)$$

where f_r represents the resonance frequency (e.g. 1.427 THz for melanoma), while Δf represents the 50% of absorption magnitude. It is important to note that the results presented in this study are based on a sample thickness of 2 µm. The quality-factor in case of normal skin, melanoma, BCC, normal breast tissue, breast cancer and normal skin when these samples were 2 µm thick are given in Table 3:

Table 3 *Quality-factor of samples at thickness of 2 µm*

Sample	Quality-factor
Normal skin	792
BCC	746.6
Melanoma	645.2
Normal breast tissue	444.1
Breast cancer	430.6

Our previous research has demonstrated that sensor sensitivity increases with greater sample thickness [31]. Consequently, an analysis of frequency shift as a function of sample thickness was conducted. Fig. 12 provides a summary of the frequency shifts observed in the detection of skin and breast cancers as the sample thickness varied. The sample thickness was changed from 2 µm to 16 µm and the difference between the peak absorption frequencies of the normal sample and the cancerous sample was calculated. For instance, the absorption peak of a normal skin sample of 4 µm was obtained at 1.425 THz, and the absorption peak of BCC of 4 µm (1.375 THz) was subtracted from it. In this way, the sensitivity based on the thickness of the sample was calculated for sample thicknesses from 2 µm to 16 µm on step of 2 µm. Fig. 12 illustrates that the sensor's sensitivity is directly proportional to the thickness of the sample. This is apparent from the larger frequency shifts observed at increased sample thicknesses. The sensor's sensitivity can be quantitatively measured by analysing the differences in the absorption peak shifts at different sample thicknesses, using (4) [32]. The relationship highlights the improved capability of the THz sensor in detecting cancerous growths as the sample thickness increases.

$$S = \frac{\Delta f_{sh} - \Delta f_{st}}{t_h - t_s}, \quad (4)$$

where Δf_{sh} and Δf_{st} are the shift in resonance for the highest and smallest thicknesses of the sample, respectively and t_h and t_s are the highest and smallest thicknesses, respectively. It is determined that the sensitivity per unit change in thickness in µm in the case of BCC is 3.7 GHz/µm and it is 5.2 GHz/µm in the case of melanoma. The smallest change in sensitivity concerning changes in thickness is obtained in the case of breast cancer where it is found to be 1.7 GHz/μm. This indicates that the shift in absorption peak will be 3.7 GHz, 5.2 GHz and 1.7 GHz if the sample size is increased by 1 μm in the case of BCC, melanoma and breast cancer, respectively.

The proposed THz metamaterial sensor achieves a significant high absorption efficiency of up to 99% and a peak spectral sensitivity of 5.2 GHz/μm, placing it among the most responsive non-invasive diagnostic platforms reported to date. Compared to existing designs, the absorber offers a compelling balance between absorption sharpness and frequency shift resolution, rivalling or surpassing prior state-of-the-art benchmarks in cancer detection using THz metamaterials.

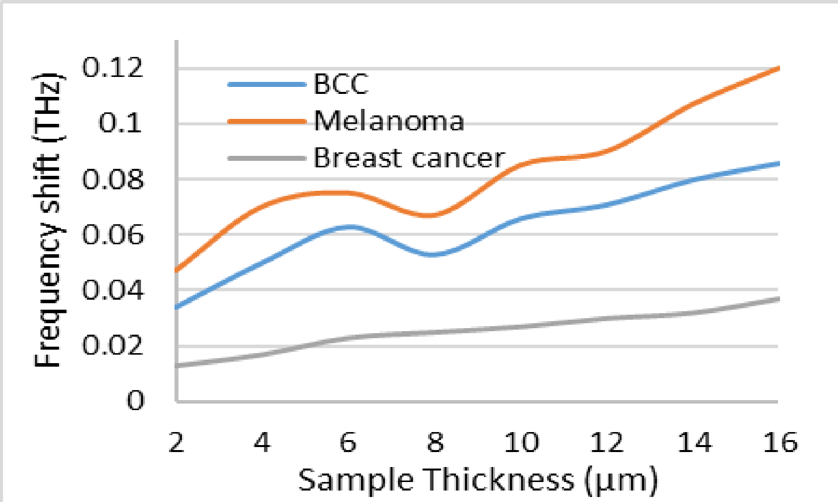

Fig. 12 *Sensitivity of the THz metamaterial absorber in terms of frequency shift as a function of sample thickness (2–16 μm)*

Further analysis of the absorber based on detailed electromagnetic properties is presented in Fig. 13. The thickness was varied from 2 μm to 16 μm and quality-factor, absorption rate and resonance frequency were analysed for each sample considered in this study. A clear trend is observed where the resonance frequency decreases with increasing tissue thickness for all samples. Cancerous tissues generally exhibit lower resonance frequencies than their corresponding normal tissues, with melanoma showing the highest initial resonance (1.728 GHz at 2 μm) and the steepest decline as thickness increases. Absorption values remain high across all tissues, typically above 0.9, but cancerous tissues, especially melanoma shows slightly higher absorption than normal tissues, indicating greater energy dissipation. The Q-factor, representing the sharpness of resonance, declines with thickness in all tissues but shows a particularly steep drop in melanoma, from 645.2 at 2 μm to as low as 4–10 at higher thicknesses. Breast cancer also exhibits significantly lower Q-factors compared to normal breast tissue. These patterns suggest that melanoma and breast cancer tissues can be distinctly identified through their higher absorption and markedly lower Q-factors, as well as more pronounced resonance shifts with thickness, highlighting their potential for differentiation using electromagnetic sensing techniques.

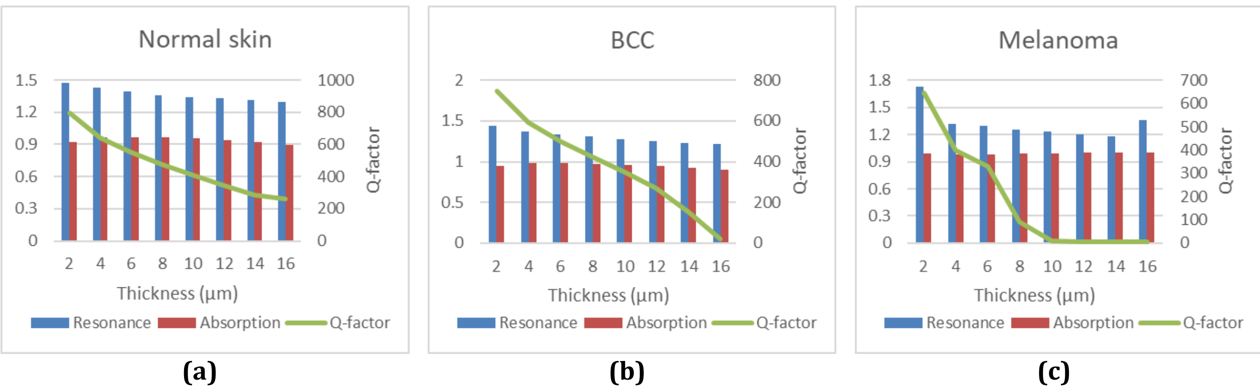

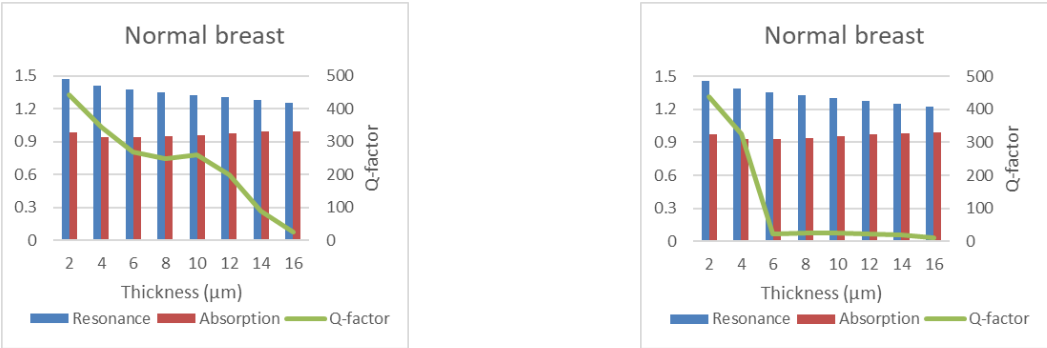

(d) **(e)**

Fig. 13 *Resonance frequency, absorption, and Q-factor at different thickness of samples (a) Normal skin; (b) BCC; (c) Melanoma; (d) Normal breast; (e) Normal breast*

A Decision Tree Classifier was implemented to classify tissue types based on simulated spectral features, namely resonance frequency, absorption magnitude, and quality factor. The dataset was derived from parametric simulations with varying tissue thicknesses and was partitioned into training and testing sets using a stratified sampling 80:20 split. An overall classification accuracy of 97.5% was achieved, with no errors observed for melanoma and BCC samples. As shown in Fig. 14, the classifier exhibited clear decision boundaries based on resonance frequency and quality factor. Although absorption was part of the full feature set and contributed to the model's accuracy, it is not depicted in the 2D plot. Feature importance analysis confirmed that resonance frequency was the most significant predictor, followed by quality factor and absorption. These findings demonstrate the potential of combining THz spectral responses with machine learning to enhance non-invasive cancer detection using metamaterial biosensors.

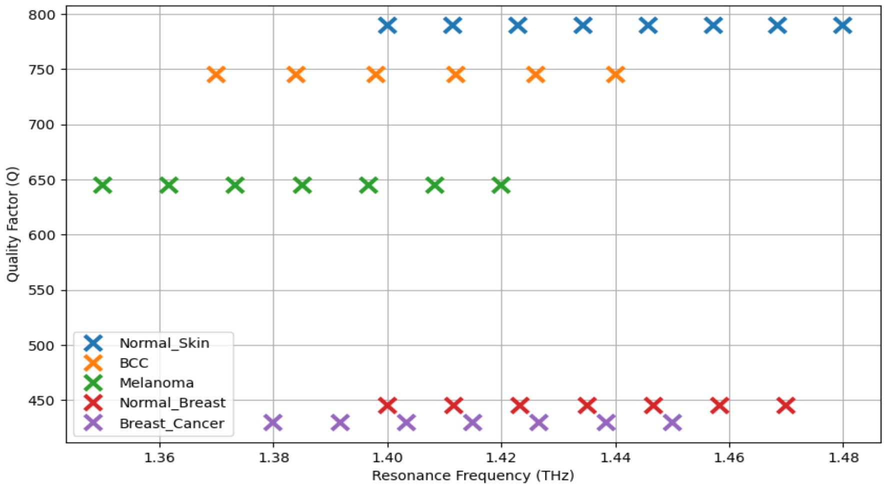

Fig. 14 *Decision boundaries generated by a Decision Tree Classifier using resonance frequency and quality factor as input features*

As summarized in Table 4, the proposed sensor demonstrates strong performance compared to previously reported THz absorbers in terms of absorption efficiency, operating frequency, and thickness-based sensitivity across different tissue types. Notably, the resonance frequencies of cancerous tissues consistently shifted to lower values compared to their healthy counterparts, with shifts of 35 GHz for BCC, 48 GHz for melanoma, and 14 GHz for breast cancer. These shifts were observed with a fixed sample thickness of 2 μm, confirming the design's capability to discriminate subtle dielectric changes. Furthermore, the sensor exhibited a linear sensitivity trend with increasing sample thickness as this is an essential characteristic for severity assessment in biomedical diagnostics. Furthermore, the quality-factor of the design also shows satisfactory results when compared to the previously presented designs. The quality-factor is found higher only in [24] that is because of their design incorporating graphene as multilayer structure. However, this results in increased design complexity. In comparison, the proposed metamaterial absorber is simple and optimum design that can help detecting cancer at early stages efficiently.

Table 4 *Benchmarking against state-of-the-Art THz absorber*

Ref.	Absorber Type	Freq. (THz)	Absorptivity	Sensitivity (GHz/μm)	Quality-factor
[33]	Graphene-infused metamaterial	4.48	99%	23.75	127
[30]	Metamaterial	0-1	99%	-	126
[24]	Graphene-based Metamaterial	6.7	99%	175	670
[34]	Metamaterial	1.6	99%	-	155.98
This work	Metamaterial	1.4	99%	5.2	645.2

4. Conclusion

A high-performance terahertz (THz) metamaterial absorber has been presented, uniquely optimized for non-invasive, ultra-sensitive detection of skin and breast cancers. The proposed absorber achieves a base absorption of 51% in the unloaded state. When loaded with biological tissue samples, the structure exhibits a substantial enhancement in absorption reaches up to 99% for melanoma and 98% for normal breast tissue driven by dielectric-induced resonance modulation.

Through full-wave simulations and Double Debye modelling of tissue dielectric properties, the sensor demonstrates significant resonance frequency shifts corresponding to malignant versus normal samples, with a peak sensitivity of 5.2 GHz/μm for melanoma detection. The observed linear correlation between sample thickness and frequency shift further reinforces the sensor's potential for early-stage cancer detection and severity assessment.

Despite being simulation-based, the sensor design is grounded in realistic fabrication materials and validated against established analytical models, showcasing strong potential for physical realization. Future efforts will focus on experimental validation using terahertz time-domain spectroscopy (THz-TDS) and the development of portable, real-time diagnostic systems, and the integration of AI-based classifiers to enable intelligent tissue recognition and automated cancer stage prediction.

This study not only underscores the viability of THz metamaterials for cancer diagnostics but also paves the way for non-invasive, label-free screening technologies that could significantly improve early detection and intervention outcomes.

Acknowledgement

This research was supported by Universiti Tun Hussein Onn Malaysia (UTHM) through TIER 1 (Vot Q447).

Conflict of Interest

Authors declare that there is no conflict of interests regarding the publication of the paper.

Author Contribution

The authors confirm contribution to the paper as follows: ***study conception and design:*** *Suhail Asghar Qureshi, Zuhairiah Zainal Abidin;* ***data collection:*** *Suhail Asghar Qureshi, Huda A. Majid;* ***analysis and interpretation of results:*** *Noor Azwan Shairi, Hongnian Yu, Nurul Bashirah binti Ghazali;* ***draft manuscript preparation:*** *Suhail Asghar Qureshi. All authors reviewed the results and approved the final version of the manuscript.*

References

[1] M. A. Naser, A. A. Majeed, M. Alsabah, T. R. Al-Shaikhli, and K. M. Kaky, "A Review of Machine Learning's Role in Cardiovascular Disease Prediction: Recent Advances and Future Challenges," Algorithms, vol. 17, no. 2, p. 78, Feb. 2024, doi: 10.3390/a17020078.

[2] M. Alsabah, M. A. Naser, A. S. Albahri, O. S. Albahri, A. H. Alamoodi, S. H. Abdulhussain, and L. Alzubaidi, "A comprehensive review on key technologies toward smart healthcare systems based IoT: technical aspects, challenges and future directions," *Artif. Intell. Rev.*, vol. 58, no. 11, p. 343, Aug. 2025, doi: 10.1007/s10462-025-11342-3.

[3] J. Wang, M. Naftaly, and E. Wasige, "An Overview of Terahertz Imaging with Resonant Tunneling Diodes,"

Appl. Sci., vol. 12, no. 8, p. 3822, Apr. 2022, doi: 10.3390/app12083822.

[4] M. Gezimati and G. Singh, “Terahertz Imaging and Sensing for Healthcare: Current Status and Future Perspectives,” *IEEE Access*, vol. 11, pp. 18590–18619, 2023, doi: 10.1109/ACCESS.2023.3247196.

[5] E. Castro-Camus, M. Koch, and D. M. Mittleman, “Recent advances in terahertz imaging: 1999 to 2021,” *Appl. Phys. B*, vol. 128, no. 1, p. 12, Jan. 2022, doi: 10.1007/s00340-021-07732-4.

[6] M. Gezimati and G. Singh, “Terahertz cancer imaging and sensing: open research challenges and opportunities,” *Opt. Quantum Electron.*, vol. 55, no. 8, p. 727, Aug. 2023, doi: 10.1007/s11082-023-04991-7.

[7] S. J. Park, S. H. Cha, G. A. Shin, and Y. H. Ahn, “Sensing viruses using terahertz nano-gap metamaterials,” *Biomed. Opt. Express*, vol. 8, no. 8, p. 3551, Aug. 2017, doi: 10.1364/boe.8.003551.

[8] V. Anitha, A. Beohar, and A. Nella, “THz Imaging Technology Trends and Wide Variety of Applications: a Detailed Survey,” *Plasmonics*, vol. 18, no. 2, pp. 441–483, Apr. 2023, doi: 10.1007/s11468-022-01775-9.

[9] Y. Roh, S.-H. Lee, J. Kwak, H. S. Song, S. Shin, Y. K. Kim, J. W. Wu, B.-K. Ju, B. Kang, and M. Seo, “Terahertz imaging with metamaterials for biological applications,” *Sensors Actuators B Chem.*, vol. 352, p. 130993, Feb. 2022, doi: 10.1016/j.snb.2021.130993.

[10] M. Mohammadiaria and S. B. Srivastava, “Metasurface-assisted bioelectronics: bridging photonic innovation with biomedical implants,” *Light Sci. Appl.*, vol. 14, no. 1, p. 386, Nov. 2025, doi: 10.1038/s41377-025-02072-w.

[11] S. Shamim, A. S. M. Mohsin, M. M. Rahman, and M. B. Hossain Bhuian, “Recent advances in the metamaterial and metasurface-based biosensor in the gigahertz, terahertz, and optical frequency domains,” *Heliyon*, vol. 10, no. 13, p. e33272, Jul. 2024, doi: 10.1016/j.heliyon.2024.e33272.

[12] Z. Vafapour, A. Keshavarz, and H. Ghahraloud, “The potential of terahertz sensing for cancer diagnosis,” *Heliyon*, vol. 6, no. 12, p. e05623, Dec. 2020, doi: 10.1016/j.heliyon.2020.e05623.

[13] R. M. Woodward, V. P. Wallace, R. J. Pye, B. E. Cole, D. D. Arnone, E. H. Linfield, and M. Pepper, “Terahertz Pulse Imaging of ex vivo Basal Cell Carcinoma,” *J. Invest. Dermatol.*, vol. 120, no. 1, pp. 72–78, Jan. 2003, doi: 10.1046/j.1523-1747.2003.12013.x.

[14] A. J. Fitzgerald, V. P. Wallace, M. Jimenez-Linan, L. Bobrow, R. J. Pye, A. D. Purushotham, and D. D. Arnone, “Terahertz Pulsed Imaging of Human Breast Tumors,” *Radiology*, vol. 239, no. 2, pp. 533–540, May 2006, doi: 10.1148/radiol.2392041315.

[15] H. Emami Nejad, A. Mir, and A. Farmani, “Supersensitive and Tunable Nano-Biosensor for Cancer Detection,” *IEEE Sens. J.*, vol. 19, no. 13, pp. 4874–4881, Jul. 2019, doi: 10.1109/JSEN.2019.2899886.

[16] M. Richter, Y. Loth, A. K. Wigger, D. Nordhoff, N. Rachinger, C. Weisenstein, A. K. Bosserhoff, and P. H. Bolívar, “High specificity THz metamaterial-based biosensor for label-free transcription factor detection in melanoma diagnostics,” *Sci. Rep.*, vol. 13, no. 1, p. 20708, Nov. 2023, doi: 10.1038/s41598-023-46876-5.

[17] N. Cui, M. Guan, M. Xu, W. Fang, Y. Zhang, C. Zhao, and Y. Zeng, “Design and application of terahertz metamaterial sensor based on DSRRs in clinical quantitative detection of carcinoembryonic antigen,” *Opt. Express*, vol. 28, no. 11, p. 16834, May 2020, doi: 10.1364/OE.393397.

[18] A. Alhegazi, Z. Zakaria, N. A. Shairi, T. Sutikno, R. A. Alahnomi, A. I. Abu-Khadrah, S. A. M. Akhir, S. Z. Ibrahim, N. Rosli, A. S. M. Zain, N. Khalid, I. Parkhomey, J. Boiko, I. Zeniv, and T. Bondarenko, “Analysis and Investigation of a Novel Microwave Sensor with High Q-Factor for Oil Sensing,” *Indones. J. Electr. Eng. Comput. Sci.*, vol. 12, no. 3, p. 1407, Dec. 2018, doi: 10.11591/ijeecs.v12.i3.pp1407-1412.

[19] H. J. Lee, J. H. Lee, S. Choi, I. S. Jang, J. S. Choi, and H. Il Jung, “Asymmetric split-ring resonator-based biosensor for detection of label-free stress biomarkers,” *Appl. Phys. Lett.*, vol. 103, no. 5, p. 053702, Jul. 2013, doi: 10.1063/1.4816440.

[20] A. Keshavarz and Z. Vafapour, “Water-Based Terahertz Metamaterial for Skin Cancer Detection Application,” *IEEE Sens. J.*, vol. 19, no. 4, pp. 1519–1524, Feb. 2019, doi: 10.1109/JSEN.2018.2882363.

[21] X. X. Xin Xu, Y. W. Yan Wu, T. H. Tangyan He, Y. L. Yuanyuan Li, F. H. Fangrong Hu, H. L. Huasheng Liang, C. Y. Chunxia Yang, and H. Z. Hong Zhong, “Metamaterials-based terahertz sensor for quick diagnosis of early lung cancer,” *Chinese Opt. Lett.*, vol. 15, no. 11, p. 111703, 2017, doi: 10.3788/COL201715.111703.

[22] S. Niknam, M. Yazdi, and S. Behboudi Amlashi, “Enhanced Ultra-Sensitive Metamaterial Resonance Sensor based on Double Corrugated Metal stripe for Terahertz Sensing,” *Sci. Rep.*, vol. 9, no. 1, p. 7516, May 2019, doi: 10.1038/s41598-019-44026-4.

[23] A. S. Saadeldin, M. F. O. Hameed, E. M. A. Elkaramany, and S. S. A. Obayya, “Highly Sensitive Terahertz Metamaterial Sensor,” *IEEE Sens. J.*, vol. 19, no. 18, pp. 7993–7999, Sep. 2019, doi:

10.1109/JSEN.2019.2918214.

[24] A. Rezazadeh and M. R. Soheilifar, “THz absorber for breast cancer early detection based on graphene as multi-layer structure,” *Opt. Quantum Electron.*, vol. 53, no. 10, p. 555, Oct. 2021, doi: 10.1007/s11082-021-03198-y.

[25] T. Matsui, S. Taniguchi, K. Yoshida, and H. Murata, “Reflection-less frequency-selective microwave metamaterial absorber,” *OSA Contin.*, vol. 4, no. 8, p. 2351, Aug. 2021, doi: 10.1364/OSAC.432737.

[26] B. C. Q. Truong, Hoang Duong Tuan, Ha Hoang Kha, and H. T. Nguyen, “Debye Parameter Extraction for Characterizing Interaction of Terahertz Radiation With Human Skin Tissue,” *IEEE Trans. Biomed. Eng.*, vol. 60, no. 6, pp. 1528–1537, Jun. 2013, doi: 10.1109/TBME.2013.2237908.

[27] B. C. Q. Truong, H. D. Tuan, A. J. Fitzgerald, V. P. Wallace, and H. T. Nguyen, “High correlation of double Debye model parameters in skin cancer detection,” in *2014 36th Annual International Conference of the IEEE Engineering in Medicine and Biology Society*, Aug. 2014, pp. 718–721. doi: 10.1109/EMBC.2014.6943691.

[28] K. Y. Chan and R. Ramer, “Novel concept of detecting basal cell carcinoma in skin tissue using a continuous-wave millimeter-wave rectangular glass filled probe,” *Med. Devices Evid. Res.*, vol. Volume 11, pp. 275–285, Aug. 2018, doi: 10.2147/MDER.S168338.

[29] R. Zhang, K. Yang, B. Yang, N. A. AbuAli, M. Hayajneh, M. Philpott, Q. H. Abbasi, and A. Alomainy, “Dielectric and Double Debye Parameters of Artificial Normal Skin and Melanoma,” *J. Infrared, Millimeter, Terahertz Waves*, vol. 40, no. 6, pp. 657–672, Jun. 2019, doi: 10.1007/s10762-019-00597-x.

[30] Y. I. Abdulkarim, O. Altintas, A. S. Karim, H. N. Awl, F. F. Muhammadsharif, F. Ö. Alkurt, M. Bakir, B. Appasani, M. Karaaslan, and J. Dong, “Highly Sensitive Dual-Band Terahertz Metamaterial Absorber for Biomedical Applications: Simulation and Experiment,” *ACS Omega*, vol. 7, no. 42, pp. 38094–38104, Oct. 2022, doi: 10.1021/acsomega.2c06118.

[31] S. Asghar Qureshi, Z. Zainal Abidin, M. R. Kamarudin, and N. B. Ghazali, “Early Detection and Quantitative Analysis of Skin Cancer Using THz Metamaterial Biosensor,” *Int. J. Integr. Eng.*, vol. 16, no. 5, Aug. 2024, doi: 10.30880/ijie.2024.16.05.021.

[32] S. K. Yee, S. C. J. Lim, P. S. Pong, and S. H. Dahlan, “MICROSTRIP DEFECTED GROUND STRUCTURE FOR DETERMINATION OF BLOOD GLUCOSE CONCENTRATION,” *Prog. Electromagn. Res. C*, vol. 99, pp. 35–48, 2020, doi: 10.2528/PIERC19110501.

[33] T. Islam and A. Eroglu, “THz Sensor Design With Graphene-Infused Metamaterial for Material Analysis,” *IEEE Trans. Magn.*, vol. 60, no. 9, pp. 1–5, Sep. 2024, doi: 10.1109/TMAG.2024.3432907.

[34] Z. EL-Wasif, T. Ismail, and O. Hamdy, “Design and optimization of highly sensitive multi-band terahertz metamaterial biosensor for coronaviruses detection,” *Opt. Quantum Electron.*, vol. 55, no. 7, p. 604, Jul. 2023, doi: 10.1007/s11082-023-04906-6.